Journal of Alloys and Compounds 743 (2018) 639–645

Contents lists available at ScienceDirect

Journal of Alloys and Compounds

journal homepage: http://www.elsevier.com/locate/jalcom

Ordered mesoporous carbon CMK-8 cathodes for high-power and long-cycle life sodium hybrid capacitors

Tuan Ngoc Phan, Min Kyung Gong, Ranjith Thangavel, Yun Sung Lee**, Chang Hyun Ko*

School of Chemical Engineering, Chonnam National University, Gwangju, 61186, Republic of Korea

ARTICLE INFO

Article history:
Received 24 November 2017
Received in revised form
31 January 2018
Accepted 1 February 2018
Available online 3 February 2018

Keywords:
Sodium hybrid capacitors
Ordered mesoporous carbon
CMK-8
Template synthesis
KIT-6
High power capacitor

ABSTRACT

Electrochemical energy storage (EES) devices with simultaneous high energy and high power output are critical in next-generation smart applications. Sodium hybrid capacitors (NHCs) are relatively new devices integrating the functions of batteries and capacitors. Research on capacitor-type carbon electrodes in NHCs is necessary to improve the energy-power behavior. Herein, we study ordered mesoporous carbon (OMC) materials synthesized at different temperatures (600 °C, 750 °C, and 900 °C) utilizing the KIT-6 silica template applied as adsorption cathodes for NHCs, paired with the superionic conductor $Na_3V_2(PO_4)_3$ as the anode material. Raman measurement indicates that the degree of graphitization is maximized at 750 °C. As a result, the OMC carbonized at 750 °C delivered the best performance among three OMCs, with a high energy density (54 W h kg^{-1}), high power (2200 W kg^{-1}) and superior stability (5000 cycles). The current research demonstrates a new platform for utilizing OMCs as adsorption electrodes in NHCs to realize a high-energy, high-power, and highly stable storage devices.

1. Introduction

The increased utilization of electrochemical energy storage (EES) devices is an obvious need in the current time of energy crises and environmental pollution. Lithium-ion batteries (LIBs) and sodium-ion batteries (NIBs) exhibit the high energy densities, which are beneficial for large-scale commercialization. However, the limited specific powers and short cycle lifetimes of LIBs and NIBs restrict their further applications [1,2]. Meanwhile, supercapacitors possess high power densities and long-term stability for a million cycles, but low energy densities because of the physical adsorption–desorption mechanism [3]. Thus, hybrid capacitors that integrate the high energy density of batteries with the superior power density and long-term stability of supercapacitors are important for the development of EES devices.

Hybrid capacitor systems utilize conventional porous carbon electrodes as the cathodes to store anions via non-faradic sorption mechanisms and battery-type intercalation anodes to store cations via redox reactions. Based on the type of cation stored in the battery electrode, these systems can be classified as lithium or sodium hybrid capacitors [4,5]. Sodium hybrid capacitors (NHCs) as emerging energy storage devices have recently been demonstrated as potential rivals to lithium hybrid capacitors (LHCs) in terms of both performance and cost. However, NHCs require deeper investigations for further improvements in their energy-power behaviors [6,7].

The energy-power behaviors of NHCs are greatly influenced by the cathodes, which are generally porous carbon materials. A large capacity difference between the anode and cathode in an asymmetric configuration can greatly affect the energy retention at high-power conditions [8–10]. The surface area and pore structure of the cathode are the critical factors affecting the charge storage capacity. Generally, a high-surface-area carbon-based material with many pores facilitates high electrochemical capacitance [11,12].

Among various carbon materials, ordered mesoporous carbon (OMC) materials have recently attracted much attention because they have well-ordered pore structures, extremely high surface areas and pore volumes, and good chemical and mechanical stability [13]. OMCs are generally synthesized by replication from mesoporous silica templates, including MCM-48 [14,15], SBA-1 [16], SBA-15 [17], and KIT-6 [18], named CMK-1, CMK-2, CMK-3, and CMK-8, respectively. By varying the pore structure of the mesoporous silica template, different types of carbon materials can be produced. Research on OMCs for NHCs is lacking to date. CMK-3, with a hexagonally ordered mesoporous structure synthesized

* Corresponding author.
** Corresponding author.
E-mail addresses: leeys@jnu.ac.kr (Y.S. Lee), chko@jnu.ac.kr (C.H. Ko).

https://doi.org/10.1016/j.jallcom.2018.02.007
0925-8388/

using SBA-15 as a template, is among the most common electrode materials [13,19,20]. Although CMK-3 possesses a high energy storage capacity, it also exhibits low structural stability and poor ion mobility [21]. The 3D cubic mesostructure KIT-6 is a better candidate than SBA-15 to synthesize carbon-based materials for supercapacitors. CMK-8, synthesized via KIT-6, is expected to have high structural stability and high ion adsorption kinetics, thereby presenting good candidacy for use as NHC cathodes.

Herein, we report for the first time the utilization of OMCs derived from KIT-6 silica templates as the cathode for NHCs coupled with $Na_3V_2(PO_4)_3$ (NVP) as a sodium insertion host (anode). OMCs synthesized at various temperatures (600 °C, 750 °C, and 900 °C) were used as capacitor-type adsorption electrodes. The effects of the carbonization temperatures, pore structures, and textural properties on the electrochemical performance of the NHCs were deeply investigated. OMC used in hybrid capacitors can greatly enhance the high-power behaviors of NHCs, while providing good cyclability. The results also suggest the need for OMCs with strong carbon frameworks to enhance the energy output, power, and cyclability of NHCs.

2. Experimental section

2.1. Synthesis of mesoporous carbon

The mesoporous silica template KIT-6 was prepared according to a procedure reported elsewhere [22]. Typically, 9.6 g of the triblock copolymer P123 (Sigma-Aldrich) was mixed with 346.6 g distilled water and 18.8 g concentrated HCl (Daejung Chemical & Metal, South Korea). After the complete dissolution of P123, 9.6 g of butanol (Sigma-Aldrich) was added. The mixed solution was then stirred for 1 h at 35 °C, followed by the addition of 24.8 g tetraethyl orthosilicate (Sigma-Aldrich) and holding at 35 °C for 24 h. The mixture was then held at 100 °C for another 24 h. The white precipitate was collected, washed by distilled water several times, and dried at 100 °C. Mesoporous KIT-6 was obtained after calcination at 550 °C for 2.5 h.

The mesoporous carbon CMK-8 was synthesized by an incipient wetness method using the KIT-6 template. A certain amount of furfuryl alcohol (Sigma-Aldrich), corresponding to 80% of the pore volume of KIT-6 was used to impregnate 3.0 g of KIT-6 template. The impregnated sample was dried at 100 °C for 6 h and heated at 350 °C for 2 h in N_2 with the heating rate of 1.3 °C/min. The impregnation process was repeated twice more with the volumes of furfuryl alcohol corresponding to 50% and 20% of the pore volume of KIT-6, respectively. After the third impregnation step, the mixture was carbonized at high temperatures of 600 °C, 750 °C, and 900 °C for 2 h in N_2 flow. The black powder obtained after carbonization was washed with a solution of 2 M NaOH and deionized water to remove the silica template and then dried at 100 °C for 12 h. The OMCs carbonized at different temperatures are henceforth denoted as CMK-*x*, where *x* is the carbonization temperature.

2.2. Characterization

The specific surface area and the total pore volume of the carbons were calculated by the N_2 adsorption–desorption measurement using a TriStar II 3020 system (Micromeritics, USA). X-ray diffraction (XRD) measurements were performed on a Rigaku D-MAX 3 system with a Cu Kβ radiation. Transmission electron microscopy (TEM) (CM200, Philips) was used to characterize the morphology and the replica of the carbon specimens. Raman spectra were recorded by a LabRam HR800 instrument (Horiba Jobin-Yvon, France, installed at Korea Basic Science Institute), equipped with an excitation laser of 515 nm in wavelength.

2.3. Electrochemical studies

Carbon-coated NVP and CMK-*x* were used as the anode and cathode in the hybrid capacitor, respectively. The synthesis methodology, structural characterization, and sodium storage ability of NVP was briefly discussed in our previous publication [6]. The half-cell performances of CMK-*x* with sodium metal as a counter electrode were shown in the supporting information (Fig. S1 and S2). The electrode composition used for the hybrid capacitor was 80 wt % of the active material, 10 wt% Ketjen black conductive additive, and 10 wt% Teflonized acetylene black binder. The slurry was cast over a stainless steel mesh under pressure and dried at 160 °C for 4 h under vacuum prior to cell fabrication. CR2032 coin-cells were assembled with NVP anodes and CMK-*x* cathodes in a standard configuration within an Ar-filled glove box with the moisture content of <0.1 ppm. The mass ratio between NVP and CMK-*x* was 1:2. The electrodes were separated by a porous polypropylene separator; the electrolyte was 1 M $NaClO_4$ in ethylene carbonate (EC)/dimethyl carbonate (DMC) (1:1 vol/vol). Cyclic voltammetry (CV) and electrochemical impedance spectroscopy (EIS) analyses were performed using a Bio-Logic electrochemical work station (SP-150, France). Galvanostatic charge–discharge studies were executed with a Won-A-Tech Battery tester (WBCS 3000, Korea) with cycling between 0 and 3 V at different current densities in ambient conditions. The power density was calculated as $P = (I \cdot V / 2\,m)$ W kg^{-1}, where I is the current, V is the working potential of the system, and m is the mass of active material in both electrodes. The energy density was calculated as $E = (P \cdot t)$ W h kg^{-1}, where t is the discharge time [6].

3. Results and discussions

3.1. Characterization of mesoporous carbon

Fig. 1 shows the XRD patterns of the KIT-6 template and CMK-*x*. In the low-angle XRD, similar to the pattern of the KIT-6 template, all patterns of CMK-*x* show three clear diffraction peaks, indexed as the (211), (220), and (420) planes of a cubic *Ia*3*d* structure [13]. These indicate the successful replication of the KIT-6 mesoporous structure. When the carbonization temperature is increased, the intensity of the main peak is increased, and all the peaks are shifted to higher degree values. These changes may be due to the structural disorder and the framework shrinkage during the carbonization process, which can cause decreases of the cell parameters [23,24]. In addition, a prominent peak appears at $2\theta = 23°$ and a small broad peak around 43° in the wide-angle XRD patterns of CMK-*x* (Fig. 1b), indicating that these materials are amorphous. The broad peak is assigned to the interlayer (002) diffraction resulting from stacks of parallel layer planes, and the intra-layer (100) peak from clusters of graphene sheets plus small amounts of disorganized carbon, respectively. The simultaneous presence of the (002) and (100) reflections suggest that CMK-*x* possess both hexagonal and rhombohedral phases [13,18,25].

The as-synthesized carbon materials were further characterized by Raman spectroscopy, as shown in Fig. 2. The Raman spectra exhibit two peaks at approximately 1340 and 1600 cm^{-1}. The first is attributed to the D band related to disordered carbon or defective graphitic structures, while the second is assigned to the G band corresponding to the typical graphitic structure [26]. Thus, higher intensity ratios of the G to D band (I_G/I_D) indicate higher degrees of graphitization. The I_G/I_D ratio is maximized at 1.29 for CMK-750 compared to CMK-600 and CMK-900, demonstrating that carbonization at 750 °C produces the carbon material with the highest-

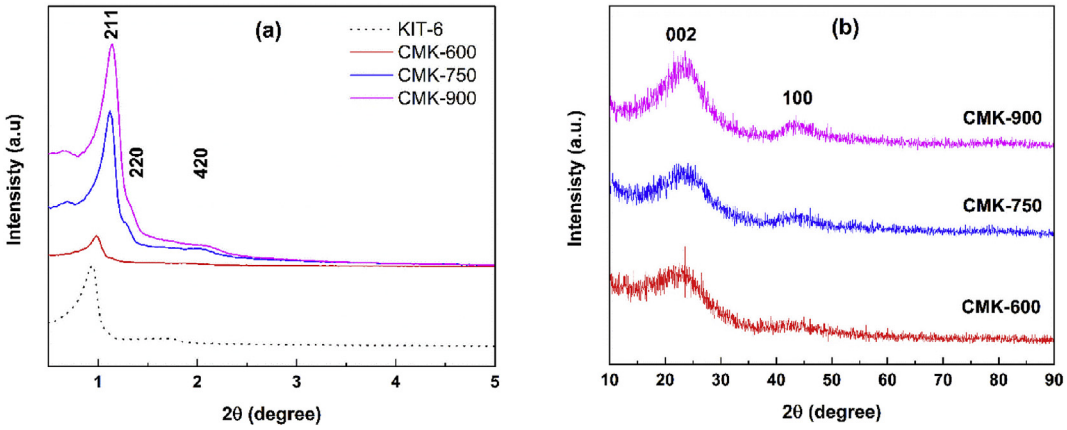

Fig. 1. (a) Low-angle and (b) high-angle XRD patterns of KIT-6 and CMK-*x*.

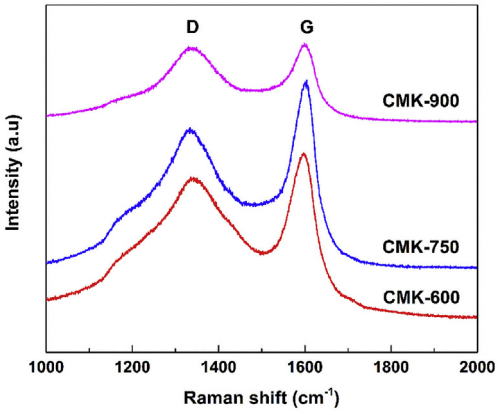

Fig. 2. Raman spectra of CMK-*x* at different carbonization temperatures.

ordered graphitic structure. When the carbonization temperature is increased to 900 °C, the I_G/I_D ratio is significantly decreased to 1.04, suggesting that structural defects arise at the highest carbonization temperature. CMK-900 contains more disordered carbon than either CMK-600 or CMK-750.

The N_2 adsorption–desorption isotherms and corresponding pore size distributions of the KIT-6 template and CMK-*x* are displayed in Fig. 3. As shown, the KIT-6 template exhibits type-IV adsorption behavior with an H1 hysteresis loop at relative pressures from 0.6 to 0.8. These features indicate a mesoporous structure with cylindrical pore geometry and high pore size uniformity [27]. After carbonization at high temperatures, the CMK-*x* specimens show H2 hysteresis loops, indicating the presence of ink-bottle mesopores. The shapes of the hysteresis loops differ somewhat depending on the carbonization temperatures. The sharper step in the isotherm of CMK-750 (0.4–0.6) compared to that of CMK-600 (0.14–0.8) indicates a more uniform mesopore structure. CMK-900 shows two distinct hysteresis loops ranging from 0.4 to 0.6 and from 0.7 to 0.99, indicating the appearance of different pore scales in this material. In addition, the pore size distribution curves of CMK-*x*, determined using the Barrett–Joyner–Halenda (BET) method (Fig. 3b), show narrow peaks that indicate uniform distributions of pore sizes in CMK-*x*. The average pore sizes of CMK-*x* are approximately 4.0–4.3 nm, much smaller than that of KIT-6. The mesopores of CMK-*x* are formed from the pore walls of the KIT-6 template, creating smaller pores in CMK-*x* compared to those in KIT-6. In addition, structural shrinkage during the high-temperature carbonization process or incomplete pore filling by carbon may contribute to the reduction in pore size [13].

The textural properties of all the samples derived from the N_2 adsorption–desorption measurements are summarized in Table 1. CMK-*x* exhibit higher specific surface areas (>900 $m^2 g^{-1}$) compared to the KIT-6 template, possibly caused by the smaller pore sizes of CMK-*x*.

The TEM images of the KIT-6 template and CMK-*x* are displayed

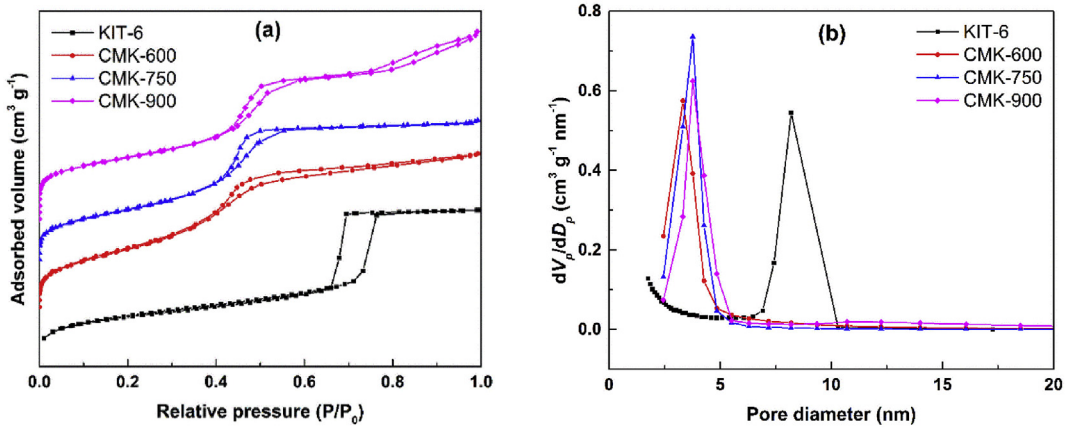

Fig. 3. (a) N_2 adsorption–desorption isotherms and (b) the pore size distributions of KIT-6 and CMK-*x*.

Table 1
Textural properties of KIT-6 and CMK-*x*.

Samples	S_{BET} ($m^2\ g^{-1}$)[a]	V_T ($cm^3\ g^{-1}$)[b]	Average pore size (nm)[c]	I_G/I_D
KIT-6	743	1.0	5.8	–
CMK-600	1090	1.1	4.0	1.14
CMK-750	944	1.0	4.2	1.29
CMK-900	979	1.2	5.1	1.04

[a] Specific surface area determined by BET equation.
[b] The total pore volume V_T was calculated at the last adsorption point ($P/P_0 = 0.99$).
[c] The average pore size was calculated by 4 V_T/S_{BET}.

in Fig. 4. All the CMK-*x* specimens clearly show well-ordered channels of *Ia*3*d* cubic structure, similar to the structure of the KIT-6 mesoporous silica. This indicates good replication of the mesostructures of the KIT-6 template. In summary, the mesoporous carbon materials prepared via a facile template synthesis method exhibit high specific surface areas, high pore volumes, and mesopores with narrow pore size distributions. These properties are generally favorable for high charge-storage performance of carbon-based materials in capacitors.

3.2. Electrochemical properties

Hybrid capacitors are constructed with CMK-*x* as the cathodes and NVP as the anodes and tested in the voltage window of 0–3 V. The mass ratio between NVP and CMK-750 is optimized to analyze the improvement in energy density (Fig. S3, S4, and S5). When the mass ratio between NVP:CMK-750 is adjusted to be 1:1, an energy density of ~62 W h kg^{-1} has been achieved at low power conditions which is higher than the cells utilizing 1:2 mass ratio. However, at high power condition of ~2.4 kW kg^{-1} it retained a much lower energy than the cells made with 1:2 ratio. This is especially due to unavailability of large number of adsorption sites in CMKs to compensate the Na insertion in NVP. In contrast, the hybrid capacitor cells with mass ratio 1:3 is not favorable due to low energy output indicating a sluggish sodium insertion in NVP. So we selected mass ratio between NVP and CMK-x = 1: 2 as a standard condition.

The CV profiles of the hybrid capacitors with various CMK-*x* are shown in Fig. 5. The CV curve profiles exhibit combinations of broad rectangles with redox peaks, deviating from the rectangular shape profile observed in electric double-layer capacitors (EDLCs). This indicates the presence of faradic reactions in the battery-type NVP electrodes and non-faradic reactions in the capacitor-type CMK-*x* electrodes. Good variations in the shape profiles and output current responses of the CV curves are observed with different CMK-*x*. CMK-750 exhibits the largest output current response among the CMK-*x* cathodes. This indicates that CMK-750 delivers better performance than CMK-600 and CMK-900. Moreover, as the scan rate increases from 1 mV s^{-1} to 10 mV s^{-1}, the shape profiles of CMK-*x* deviate from the original shapes to larger ones, because of the higher electrochemical polarization present at higher scanning rates.

Fig. 6 shows the galvanostatic charge–discharge curves of CMK-*x* measured at various current densities. The charge–discharge curves of the NHCs are not linear, but instead show combinations of plateaus and sloping lines, confirming multiple energy storage behaviors and showing good agreement with the CV profiles [28]. The charge storage behavior mainly involves sodium insertion and extraction in NVP by faradic reactions and surface ClO_4 anion adsorption and desorption over CMK-*x* by non-faradic reactions. Because CMK-*x* are high-surface-area mesoporous carbons with wider pores (>4 nm), larger numbers of active sites may be available for active ion adsorption and desorption. Furthermore, the kinetics of the energy storage reaction in NHCs are dramatically affected by the textural and structural properties of CMK-*x*. The discharge times of NHCs with different CMK-*x* at low current densities are nearly equal. However, the performance of CMK-750 is superior to that of CMK-600 and CMK-900 at higher current rates. CMK-750 not only delivers a higher discharge time but also withstands longer discharge times at higher current densities with a

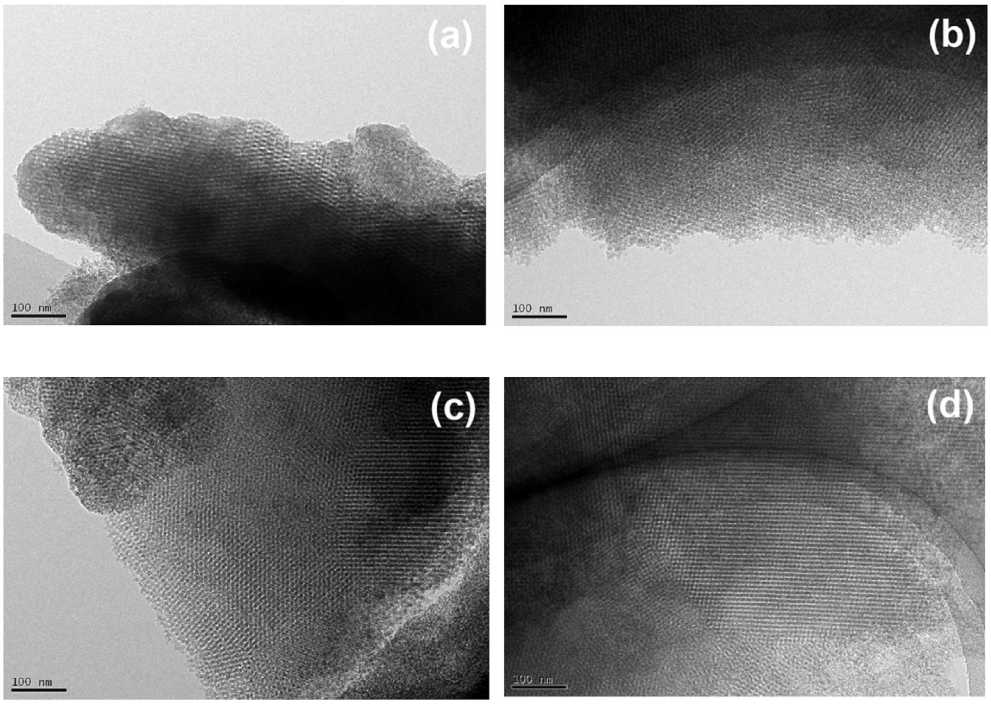

Fig. 4. TEM images of (a) KIT-6, (b) CMk-600, (c) CMK-750, and (d) CMK-900.

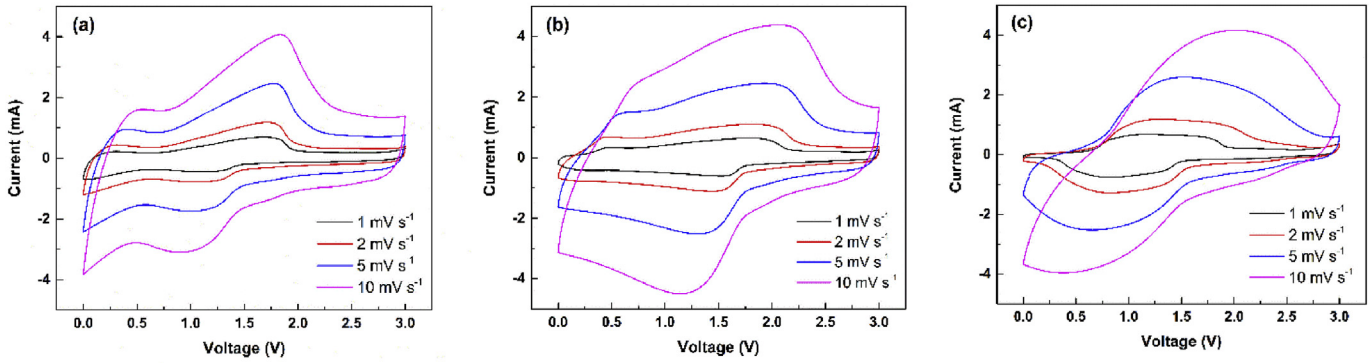

Fig. 5. CVs of (a) CMK-600, (b) CMK-750, and (c) CMK-900 at different scan rates.

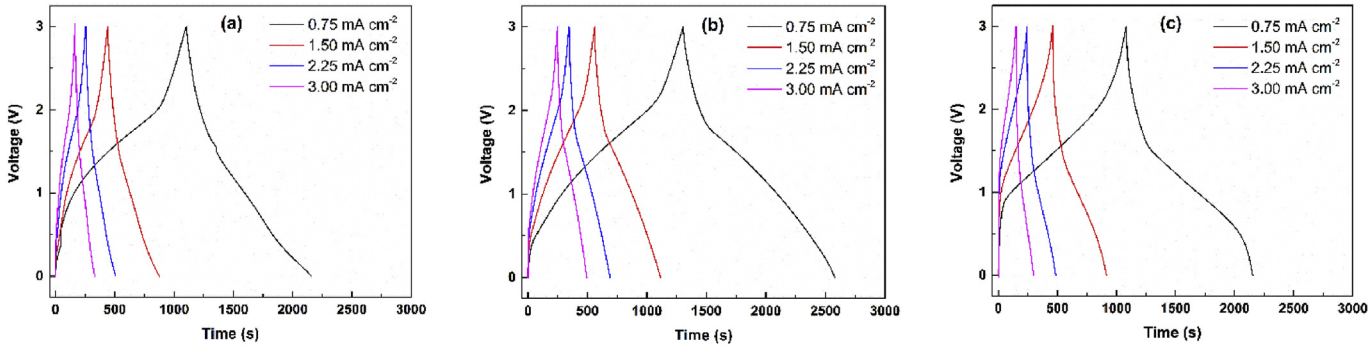

Fig. 6. Galvanostatic charge–discharge curves of (a) CMK-600, (b) CMK-750, and (c) CMK-900 at various current densities.

lower IR drop than those shown by CMK-600 and CMK-900.

All the CMK-*x* have similar specific surface areas of >900 $m^2 g^{-1}$ and total pore volumes >1.0 $cm^3 g^{-1}$, as shown in Table 1. Therefore, the only difference between these samples is the degree of graphitization, as obtained by Raman analysis; graphitization is strongly dependent on the carbonization temperature. Higher proportions of graphite in carbon materials correspond to higher electrical conductivities, causing better electrochemical performances in the carbon materials as well [19,29–31] Thus, the superior performance of CMK-750 as a cathode material for NHCs may arise from its having the highest proportion of ordered graphitic structure. The low degree of graphitization in CMK-600 attained at the lowest carbonization temperature could reduce the anionic adsorption kinetics at high current rates. As the carbonization temperature is increased, the growth of graphitic carbon in CMK-750 increases the electrical conductivity, which benefits fast adsorption and desorption reactions over the pores of the carbon. With a further increase in the carbonization temperature, the degree of carbonization is decreased for CMK-900. This means that the structural defects induced by the higher carbonization temperature cause a severe Ohmic drop and significant ion diffusional losses during the adsorption reactions.

The cyclic stabilities of the NHCs were evaluated at 0.525 mA cm^{-2} (Fig. 7a). CMK-750 retains ~70% of its initial performance after 5000 cycles, the best stability among the three investigated materials. CMK-600 possesses the lowest retention of ~50%, while CMK-900 delivers a retention of ~60% after 5000 cycles. The highest stability of CMK-750 is attributed to the highest graphitization degree that can withstand continuous adsorption and desorption reactions. The highly interconnected and strong carbon frameworks retain the porous nature of CMK-750 for longer cycling. The large mesopore content of CMK-750 may act as an electrolyte reservoir and provide short ion transfer pathways during the adsorption and desorption processes.

To elucidate the excellent performance of CMK-750, Nyquist plots of the NHCs are recorded using EIS. The Nyquist plots of all NHCs show high-frequency semicircles, assigned to charge-transfer reactions, and inclined lines in the low-frequency regions assigned to Warburg tails from the diffusion limitations of sodium ions in NHCs. The internal resistance comprises the intrinsic resistance of the mesoporous carbon materials, the resistance of the bulk electrolyte, and the resistance at the electrode–electrolyte interface. CMK-900 exhibits the largest semicircle in the high-frequency region among the three tested OMCs, indicating the highest charge-transfer resistance arising from the highly disordered pores. CMK-750 delivers the lowest internal resistance because of its highly graphitic structure, which favors the retention of high energy at high-power conditions.

The Ragone plots in Fig. 8 show the energy and power densities of NHCs made with different CMK-*x*. A high energy density of ~54 W h kg^{-1} (based on the mass of both electrodes) is delivered by CMK-750, which is higher than the energy densities delivered by NHCs with CMK-600 and CMK-900. Furthermore, the facile ion storage kinetics in CMK-750 allows the maximum power of 2200 W kg^{-1} with high energy retention, while the other CMKs deliver poor power–energy behaviors. The remarkable performance of CMK-750 is attributed to the high degree of graphitization and the strong carbon frameworks, which can withstand repeated anion adsorption; thereby, the NHC is highly stable when compared to those with the less graphitized CMK-600 and CMK-900 electrodes, and shows high energy retention at high power conditions.

The observed energy densities and powers of NHCs based on

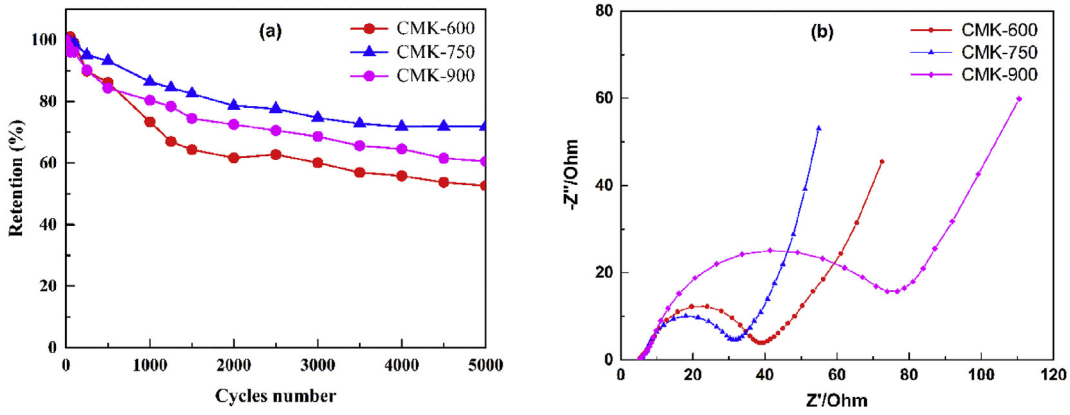

Fig. 7. (a) Cyclic performance of CMK-*x* at a current density of 0.7 A g^{-1}, and (b) Nyquist plots of CMK-*x*.

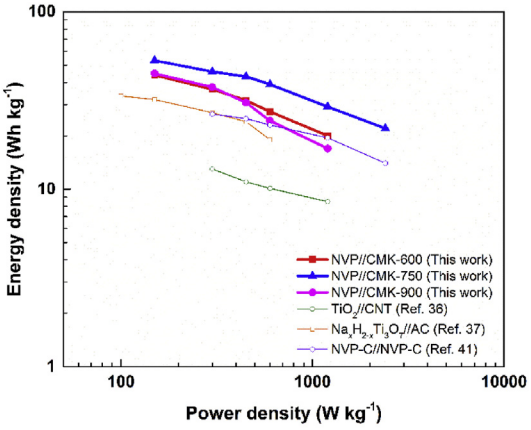

Fig. 8. Ragone plots of NHCs with CMK-*x* cathodes carbonized at different temperatures in comparison with TiO_2//CNT (carbon nanotubes), $Na_xH_{2-x}Ti_3O_7$//AC and NVP-C// NVP-C hybrid capacitors.

CMK-*x* are also higher than those of LHCs based on $Li_4Ti_5O_{12}$ [32], TiO_2 [33], V_2O_5 [34], and $Li_3V_2(PO_4)_3$ [35]. In addition, the performances of these capacitors are superior to those of several other NHC systems such as TiO_2 [36], $Na_xH_{2-x}Ti_3O_7$ [37], $Na_2Ti_3O_7$ [38,39], and NVP-C [39–41], which generally use carbon-type adsorption cathodes. The improved performance of the NHCs is mainly attributed to the large number of mesopores with the ordered structure of CMK-*x* providing more sites for active anion adsorption and fast anion adsorption, which is synergistically boosted by fast sodium insertion in the sodium superionic conductor-type NVP anode.

4. Conclusions

In summary, we have demonstrated the possibility of utilizing OMCs derived from a KIT-6 silica template as adsorption-type capacitor electrodes in NHCs when paired with NVP anodes. The results confirmed that the performances of the NHCs were strongly influenced by the structural and textural properties of the CMK-*x* cathodes. CMK-750 showed a mesoporous structure with a high level of graphitization and delivered superior performance in NHCs compared to the less graphitized CMK-600 and CMK-900. The highly carbonized mesoporous CMK-750 showed a low internal resistance and thereby favored fast ion transport within the pores, along with showing low diffusion losses. This kinetically enhanced the performance at high-current conditions and facilitated high energy retention at high-power conditions. NHCs constructed with CMK-750 and NVP showed high energy densities of 54 W h kg^{-1} along with high power density (2400 W kg^{-1}) and superior stability for 5000 cycles, outperforming several previously reported lithium and sodium hybrid capacitors. The results demonstrate that mesopores and the degree of graphitization in carbon structures are critical in improving the electrochemical performances of energy storage devices.

Acknowledgment

This work was supported by the National Research Foundation of Korea (NRF) grant funded by the Korea government (Ministry of Science, ICT & Future Planning) (No. 2016R1A4A1012224).

Appendix A. Supplementary data

Supplementary data related to this article can be found at https://doi.org/10.1016/j.jallcom.2018.02.007.

References

[1] S. Zhang, C. Li, X. Zhang, X. Sun, K. Wang, Y. Ma, High performance lithium–ion hybrid capacitors employing Fe_3O_4–graphene composite anode activated carbon cathode, ACS Appl. Mater. Interfaces 9 (2017) 17136–17144.
[2] J. Chen, X. Zhou, C. Mei, J. Xu, S. Zhou, C.P. Wong, Evaluating biomass–derived hierarchically porous carbon as the positive electrode material for hybrid Na–ion capacitors, J. Power Sources 28 (2017) 48–55.
[3] G. Tang, L. Cao, P. Xiao, Y. Zhang, H. Liu, A novel high energy hybrid Li–ion capacitor with a three–dimensional hierarchical ternary nanostructure of hydrogen–treated TiO_2 nanoparticles/conductive polymer/carbon nanotubes anode and an activated carbon cathode, J. Power Sources 355 (2017) 1–7.
[4] J.R. Rani, R. Thangavel, S.I. Oh, J.M. Woo, N.C. Das, S.Y. Kim, Y.S. Lee, J.H. Jang, High volumetric energy density hybrid supercapacitors based on reduced graphene oxide scrolls, ACS Appl. Mater. Interfaces 9 (2017) 22398–22407.
[5] V. Aravindan, J. Gnanaraj, Y.S. Lee, S. Madhavi, Insertion–type electrodes for nonaqueous Li–ion capacitors, Chem. Rev. 114 (2014) 11619–11635.
[6] R. Thangavel, K. Kaliyappan, D.-U. Kim, X. Sun, Y.-S. Lee, All-organic sodium hybrid capacitor: a new, high-energy, high-power energy storage system bridging batteries and capacitor, Chem. Mater. 29 (2017) 7122–7130.
[7] J. Ding, H. Wang, Z. Li, K. Cui, D. Karpuzov, X. Tan, A. Kohandehgahn, D. Mitlin, Peanut shell hybrid sodium ion capacitor with extreme energy–power rivals lithium ion capacitors, Energy Environ. Sci. 8 (2015) 941–945.
[8] T. Lin, I.W. Chen, F. Liu, C. Yang, H. Bi, F. Xu, F. Huang, Nitrogen–doped mesoporous carbon of extraordinary capacitance for electrochemical energy storage, Science 350 (2015) 1508–1513.
[9] L. Deng, W. Zhong, J. Wang, P. Zhang, H. Fang, L. Yao, X. Liu, X. Ren, Y. Li, The enhancement of electrochemical capacitance of biomass–carbon by pyrolysis of extracted nanofibers, Electrochim. Acta 228 (2017) 398–406.
[10] M.K. Sahoo, P. Gogoi, G. Rajeshkhanna, S.V. Chilukuri, G.R. Rao, Significance of optimal N–doping in mesoporous carbon framework to achieve high specific capacitance, Appl. Surf. Sci. 418 (2017) 40–48.
[11] R. Thangavel, B. Moorthy, D.K. Kim, Y.S. Lee, Pushing the energy output and

cyclability of sodium hybrid capacitors at high power to new limits, Adv. Energy Mater. 7 (2017) 1602654–1602663.
[12] R. Thangavel, K. Kaliyappan, H.V. Ramasamy, X. Sun, Y.S. Lee, Engineering the pores of biomass–dericed carbon: insights for achieving ultrahigh stability at high power in high–energy supercapacitors, ChemSusChem 10 (2017) 2805–2815.
[13] D. Zhang, Y. Hao, L. Zheng, Y. Ma, H. Feng, H. Luo, Nitrogen and sulfur co–doped ordered mesoporous carbon with enhanced electrochemical capacitance performance, J. Mater. Chem. A 1 (2013) 7584–7591.
[14] S. Inagaki, T. Nakao, T. Miki, N. Kuroda, Y. Kubota, Ni–catalyzed carbonization of furfuryl alcohol polymer in ordered mesoporous silica MCM-48 giving ordered mesoporous carbon CMK-1 with high electric double–layer capacitance, Microporous Mesoporous Mater. 241 (2017) 123–131.
[15] R. Ryoo, S.H. Joo, S. Jun, Synthesis of highly ordered carbon molecular sieves via template–mediated structural transformation, J. Mater. Chem. B 103 (1999) 7743–7746.
[16] S.H. Joo, S.J. Choi, I. Oh, J. Kwak, Z. Liu, O. Terasaki, R. Ryoo, Ordered nanoporous arrays of carbon supporting high dispersions of platinum nanoparticles, Nature 412 (2001) 169–172.
[17] S. Jun, S.H. Joo, R. Ryoo, M. Kruk, M. Jaroniec, Z. Liu, T. Ohsuna, O. Terasaki, Synthesis of new, nanoporous carbon with hexagonally ordered mesostructure, J. Am. Chem. Soc. 122 (2000) 10712–10713.
[18] M. Lezanska, J. Wloch, G. Szymanski, I. Szpakowska, J. Kornatowski, Properties of CMK-8 carbon replicas obtained from KIT-6 and pyrrole at various contents of ferric catalyst, Catal. Today 150 (2010) 77–83.
[19] S. Inagaki, Y. Yokoo, T. Miki, Y. Kubota, Improvement of electric double–layer capacitance of ordered mesoporous carbon CMK-3 by partial graphitization using metal oxide catalysts, Microporous Mesoporous Mater. 179 (2013) 136–143.
[20] V.C. Almeida, R. Silva, M. Acerce, O.P. Junior, A.L. Cazetta, A.C. Martins, X. Huang, M. Chhowalla, T. Asefa, N–doped ordered mesoporous carbons with improved charge storage capacity by tailoring N–dopant density with solvent–assisted synthesis, J. Mater. Chem. A 2 (2014) 15181–15190.
[21] J. Hu, M. Noked, E. Gillette, Z. Gui, S.B. Lee, Capacitance behavior of ordered mesoporous carbon/Fe_2O_3 composites: comparison between 1D cylindrical, 2D hexagonal, and 3D bicontinuous mesostructures, Carbon 93 (2015) 903–914.
[22] M. Kruk, M. Jaroniec, C.H. Ko, R. Ryoo, Characterization of the porous structure of SBA-15, Chem. Mater. 12 (2000) 1961–1968.
[23] J. Park, Y. Nabae, T. Hayakawa, M. Kakimoto, Highly selective two-electron oxygen reduction catalyzed by mesoporous nitrogen–doped carbon, ACS Catal. 4 (2014) 3749–3754.
[24] K. Xia, Q. Gao, C. Wu, S. Song, M. Ruan, Activation, characterization and hydrogen storage properties of the mesoporous carbon CMK-3, Carbon 45 (2007) 1989–1996.
[25] M. Ignat, C.J.V. Oers, J. Vernimmen, M. Mertens, S.P. Vermaak, V. Meynen, E. Popovici, P. Cool, Textural property tuning of ordered mesoporous carbon obtained by glycerol conversion using SBA-15 silica as template, Carbon 48 (2010) 1609–1618.
[26] R. Thangavel, A. Samuthira Pandian, H.V. Ramasamy, Y.-S. Lee, Rapidly synthesized, few-layered pseudocapacitive SnS2 anode for high-power sodium ion batteries, ACS Appl. Mater. Interfaces 9 (2017) 40187–40196.
[27] M. Kruk, M. Jaroniec, Gas adsorption characterization of ordered organic–inorganic nanocomposite materials, Chem. Mater. 13 (2001) 3169–3183.
[28] K. Karthikeyan, S. Amaresh, V. Aravindan, H. Kim, K.S. Kang, Y.S. Lee, Unveiling organic–inorganic hybrids as a cathode material for high performance lithium–ion capacitors, J. Mater. Chem. A 1 (2013) 707–714.
[29] Y.A. Kim, H. Kakegawa, K. Fujisawa, D. Shimamoto, H. Muramatsu, J.H. Kim, Y.C. Jung, T. Hayashi, M. Endo, M. Terrones, M.S. Dresselhaus, Sensitive G–band Raman features for the electrical conductivity of multi–walled carbon nanotubes, J. Nanosci. Nanotechnol. 10 (2010) 3940–3944.
[30] J. Li, E. Fiset, J. Yang, P. Yuan, X. Ling, D.H. Jurcakova, C. Yu, L. Wang, Formation of graphitic tubules from ordered mesoporous carbon and their effect on supercapacitive energy storage, J. Mater. Chem. 22 (2012) 21472–21480.
[31] A. Eftekhari, Z. Fan, Ordered mesoporous carbon and its applications for electrochemical energy storage and conversion, Mater. Chem. Front. 1 (2017) 1001–1027.
[32] H.G. Jung, N. Venugopal, B. Scrosati, Y.K. Sun, A high energy and power density hybrid supercapacitor based on an advanced carbon–coated $Li_4Ti_5O_{12}$ electrode, J. Power Sources 221 (2013) 266–271.
[33] H. Wang, C. Guan, X. Wang, H.J. Fan, A high energy and power Li–ion capacitor based on a TiO_2 nanobelt array anode and a graphene hydrogel cathode, Small 11 (2015) 1470–1477.
[34] V. Aravindan, Y.L. Cheah, W.F. Mak, G. Wee, B.V.R. Chowdari, S. Madhavi, Fabrication of high energy–density hybrid supercapacitors using electrospun V_2O_5 nanofibers with a self–supported carbon nanotube network, ChemPlusChem 77 (2012) 570–575.
[35] J. Jiang, G. Tan, S. Peng, D. Qian, J. Liu, D. Luo, Y. Liu, Electrochemical performance of carbon–coated $Li_3V_2(PO_4)_3$ as a cathode material for asymmetric hybrid capacitors, Electrochim. Acta 107 (2013) 59–65.
[36] Q. Wang, Z.H. Wen, J.H. Li, A hybrid supercapacitor fabricated with a carbon nanotube cathode and a TiO_2-B nanowire anode, Adv. Funct. Mater. 16 (2006) 2141–2146.
[37] J. Yin, L. Qi, H. Wang, Sodium titanate nanotubes as negative electrode materials for sodium–ion capacitors, ACS Appl. Mater. Interfaces 4 (2012) 2762–2768.
[38] S. Dong, L. Shen, H. Li, P. Nie, Y. Zhu, Q. Sheng, X. Zhang, Pseudocapacitive behaviours of $Na_2Ti_3O_7$@CNT coaxial nanocables for high-performance sodium-ion capacitors, J. Mater. Chem. A 3 (2015) 21277–21283.
[39] V. Aravindan, M. Ulaganathan, S. Madhavi, Research progress in Na-ion capacitors, J. Mater. Chem. A 4 (2016) 7538–7548.
[40] K. Sakaushi, E. Hosono, G. Nickerl, T. Gemming, H. Zhou, S. Kaskel, J. Eckert, Aromatic porous-honeycomb electrodes for a sodium-organic energy storage device, Nat. Commun. 4 (2013) 1485–1491.
[41] Z. Jian, V. Raju, Z. Li, Z. Xing, Y.S. Hu, X. Ji, A high–power symmetric Na–ion pseudocapacitor, Adv. Funct. Mater. 25 (2015) 5778–5785.